Received: 18 April 2025 | Revised: 13 June 2025 | Accepted: 23 June 2025 | Published online: 14 July 2025

RESEARCH ARTICLE

Journal of Optics and Photonics Research
2025, Vol. 00(00) 1–7
DOI: 10.47852/bonviewJOPR52025955

BON VIEW PUBLISHING

Redshift of Quantum-Particle Plasmon Stemming from Thermal-Induced Quantum Size Effects: Numerical Modeling and Experimental Evidence

Mufei Xiao[1,*], Constanza Koop-Santa[2] and Nikifor Rakov[3]

[1]*Centro de Nanociencias y Nanotecnología, Universidad Nacional Autónoma de México, Mexico*

[2]*Escuela de Ingeniería y Ciencias, Tecnologico de Monterrey, Mexico*

[3]*Universidade Federal do Vale do São Francisco, Brazil*

Abstract: Work is reported on thermal-induced redshifts of quantum particle plasmon. The redshifts are predicted to be caused indirectly by the quantum size effects. The particles are enlarged when temperature increases, and consequently, quantum size effects modify the plasmon but not the band structure. It has been modeled for metallic quantum particles. The results are also instructive to other quantum systems, such as complex molecules. Every electron inside the quantum particle is taken into account. Tiny quantum size effects are harvested, and the redshift becomes significant. What is shifted is the so-called small particle plasmon frequency, which stems from collective intraband transitions of electrons. Interband transitions are excluded from the plasmonics. Therefore, the band structure is intact from the onset. Experimental observation is also reported for the spectral redshift. Faujasite zeolites were synthesized. Optical spectroscopy has been carried out, and the resulting spectra showed a significant redshift with the increase in temperature. The experimental observation provides early phenomenological evidence for the spectral redshift predicted by our theoretical model calculations.

Keywords: quantum particle, quantum size effects, redshift, zeolites, optical spectroscopy

1. Introduction

There has been a lack of attention on the spectral dependence on temperature for quantum particles, though remotely related work appears from time to time [1–10]. Here, a quantum particle is referred to as a metallic or semiconductor particle with a dimension so tight that quantum confinement has to be taken into account. To some extent, the concept of quantum particles can be generalized to include all kinds of tiny quantum systems, such as a complex molecule. Although in situ microscopy can be realized for individual particles or molecules with near-field optical microscopy [7–22], spectroscopy of single quantum particles has been challenged or unreliable [23–28]. Theoretical modeling taking into account quantum size effects is also obstructed as there are too many electrons in a quantum particle. One often resorts to mathematics for summation rules, that is, to convert the summation into an integral. However, the tiny quantum size effects are usually smeared out due to the conversion.

Recently, with a parallel supercomputer, we demonstrated that it was possible to simultaneously take into account both the quantum size and Fermi-Dirac statistics effects in modeling quantum particles without any sum rules or integration [29]. As far as temperature dependence is concerned, one considers only the thermal-induced quantum size effects, as the Fermi-Dirac statistics brought about far less significant changes [30]. When the samples are heated, the particles expand in size, and the quantum mechanical solution changes. Since the so-called quantum size effects are rather small, the overall band structures are not modified significantly. Instead, fluctuations due to electron flows can be observed. In other words, the quantum size effects stem from the intraband transits, not the interband transits.

In the present work, we have studied the so-called small particle plasmon frequency. We have found that the plasmon frequency appears redshifted when the particles are enlarged slightly. The redshift is observable and usually a function of the increase in the size of the particle. One assumes that the size of the quantum particle is increased when the sample is heated. In passing we take note of the word redshift. Usually, redshift refers to a decrease in frequency. When the size of a quantum particle is reduced, the plasmon moves to a higher frequency, that is, a blueshift. Although if the size of the quantum particle increases due to higher temperature, the plasmon moves to a lower frequency, which indicates a redshift. The word redshift used in the present work refers to a rise in temperature that causes a spectral move towards a lower frequency.

In the present work, we also demonstrate experimental evidence of the redshift. As already mentioned, in situ spectroscopy of individual quantum particles remains challenged [23–28]. We make use of a sample that is composed of a large number of complex molecules. The sample we used belongs to the family of

*Corresponding author: Mufei Xiao, Centro de Nanociencias y Nanotecnología, Universidad Nacional Autónoma de México, Mexico. Email: mufei@ens.cnyn.unam.mx

faujasite zeolites [30]. Zeolites are mesoscopic porous materials and are widely used for catalysis. We synthesized the samples with a sol-gel technique [30]. The samples underwent many examinations with most conventional tools, such as XRD (X-ray diffraction), EDS (Energy Dispersive Spectroscopy), SEM (Scanning Electron Microscopy), and TEM (Transmission Electron Microscopy). The SEM and TEM images showed that a group of zeolite cells form agglomerates ~1.39 μm in size and the agglomerates construct layers whose thickness is ~0.12 μm. Optical spectroscopy in the ultraviolet and visible range has been carried out. Based on the resulting Tauc plots, the band gaps can be estimated. The direct and indirect band gaps were assessed to be 4.35 eV and 3.12 eV respectively. We have observed a significant redshift of the spectral band when the materials are heated up to 450 °C. Two spectra were recorded for the same sample at two different calcination temperatures, 90 and 450 °C, respectively. The structure and shape of the two spectra remain intact. However, the entire spectra have a redshift from 90 to 450 °C. The redshift is significant and overt at a peak near 245 nm. The shift measures about 5 nm. We believe that this redshift is related to the redshift predicated in our numerical modeling. It provides a piece of early phenomenological experimental evidence for the thermal redshift of quantum size effects, though the evidence may not be accurate and direct.

The rest of the paper is organized as follows. In Section 2, the theory and modeling procedures are introduced and outlined. Numerical results are presented to demonstrate the quantum size effects. In Section 3, a piece of experimental evidence is shown. A sample of faujasite zeolites is synthesized. The optical spectroscopic results for different calcination temperatures were presented, which demonstrated the redshift. The possible mechanism for the redshift is discussed. The paper is concluded in Section 4.

2. Theoretic Outlines and Numerical Modeling

To manifest the quantum size effects on quantum particles, we calculate plasmon of quantum particles, more specifically the small particle plasmon of the quantum particles. Before presenting the formalism, let us briefly introduce some relevant terms as there exist confusion and inconsistencies.

One often learns about two terms, namely the surface plasmon and the localized surface plasmon. The surface plasmon, propagating or localized, does not exist in quantum particles simply because the particles are too small. Or it needs a new name for the plasmon. Instead, there exist the so-called small particle plasmons. We show below quantitative values of each plasmon, that is, the reduced value for the surface plasmon from the bulk plasmon, and the reduced value for the small particle plasmon from the bulk plasmon. Another common confusion needs to be clarified. Interband transitions are not a part of plasmonics. Interband transitions in quantum systems are responsible for spontaneous emission, stimulated emission, and quantum absorption. On the other hand, plasmon stems from collective movements of plasmas, that often is the electrons. Therefore, for quantum particles, the plasmon stems from intraband transitions, or electrons move within an energy level.

2.1. Bulk plasmon, surface plasmon, and small particle plasmon

Plasmon may be excited in all conducting media, such as plasmas, metals, and semiconductors. Basic formalism can be found in textbooks as well as in literature (see for instance reference [31], readers are also referred to references [29, 32] for notations). The angular frequency of bulk plasmon ω_p can be estimated from

$$\omega_p^2 = \frac{(n_0 e^2)}{(m\varepsilon_0)} \tag{1}$$

where n_0 is the density of the electron, e the charge of an electron, and m the mass of an electron, respectively, and ε_0 the permittivity in a vacuum. It is well-known that light cannot excite bulk plasmon. However, at a metal-dielectric interface, surface plasmons can be excited. The frequency of surface plasmon can be related to the frequency of bulk plasmon as follows. The s-polarized reflection coefficient can be written as

$$r_s(\omega) = \frac{(\varepsilon(\omega) - 1)}{\varepsilon(\omega) + 1} \tag{2}$$

where it is assumed that the dielectric is a vacuum or in air and therefore $\varepsilon(\omega) = 1$. The relative dielectric function of the metal $\varepsilon(\omega)$ can be related to the plasmon frequency with the Drude model as

$$\varepsilon(\omega) = 1 - \frac{\omega_p^2}{(\omega^2 + i\omega\gamma)} \tag{3}$$

where γ represents a damping coefficient. Combining Equations (2) and (3), one understands that the maximum or resonant reflection takes place when the denominator of the reflection coefficient in Equation (2) tends to zero or the minimum, which requires $\omega_{sf} \approx \omega_p/\sqrt{2}$, where ω_{sf} is referred to as the angular frequency of the surface plasmon. It demonstrates that the frequency of surface plasmon is lower than the frequency of bulk plasmon $\omega_{sf} \approx 0.7\omega_p$.

For small metallic particles, surface plasmons exist also at the boundary. Since the particle is small, the surface plasmon polaritons are highly localized, as a standing wave, and therefore surface plasmons of small particles are often referred to as the localized plasmon. For quantum particles, the localized plasmon needs a new name, the small particle plasmon. However, the frequency of small particle plasmon for the quantum particles appears at a lower value. To understand the small particle plasmon, one starts from the Rayleigh polarizability for subwavelength spherical particles of radius a as

$$\alpha(\omega) = 4\pi\varepsilon_0 a^3 \frac{\varepsilon(\omega) - 1}{\varepsilon(\omega) + 2} \tag{4}$$

Combining the Drude model in Equations (3) and (4), one shows that the resonant absorption and also the strongest scattering takes place when the denominator in Equation (4) tens to zero or the minimum. Consequently $\omega_{sp} \approx \omega_p/\sqrt{3}$, this can be referred to as the small particle plasmon frequency. The frequency of small particle plasmon is even lower than the frequency of surface plasmon $\omega_{sp} \approx 0.577\omega_p$.

Note that, based on the results from our numerical modeling, the plasmon frequency of small particles is always near $\omega_{sp} \approx 0.577\omega_p$, away from the frequency of surface plasmon $\omega_{sf} \approx 0.7\omega_p$.

2.2. Solutions of Schrödinger equation for infinite spherical quantum well

In the present work, fluctuations of the frequency and strength of small particle plasmon stemming from quantum confinement are extensively studied. These are tiny fluctuations. Harvesting all changes, one obtains noticeable quantum size effects. Without considering the quantum confinement, there is implicitly an assumption that the density of electrons is a constant inside the particle, i.e., the electrons are uniformly distributed everywhere. The assumption becomes questionable when the quantum confinement has to be considered because of quantum mechanics.

In turn, variant electron density induces a variant dielectric function. The polarizability of the particle becomes an integral over the particle volume as

$$\alpha(\omega) = 3\varepsilon_0 \iiint_v \frac{\varepsilon(r,\omega)-1}{\varepsilon(r,\omega)+2} d^3r \tag{5}$$

For spherical particles, only the radial coordinator brings about changes. One eventually has

$$\alpha(\omega) = 12\pi\varepsilon_0 \int_0^a \frac{\varepsilon(r,\omega)-1}{\varepsilon(r,\omega)+2} r^2 dr \tag{6}$$

where a indicates the radius of the sphere. The source of the variation in the dielectric function $\varepsilon(r,\omega)$ stems from the fluctuation in electron density $n(r)$. Combining Equations (1) and (3), one writes down immediately the modified dielectric function as

$$\varepsilon(r,\omega) = 1 - \frac{\omega_p^2 n(r)/n_0}{\omega^2 + i\omega\gamma} \tag{7}$$

where the electron density $n(r)$ is normalized to the constant electron density n_0 of the bulk material. Therefore, the next task to deal with quantum particles is to calculate $n(r)/n_0$ with a computable quantum mechanics model. The simplest quantum mechanical model is the electron-in-a-box model. All electrons are confined within an infinite spherical quantum well. Solutions of the time-independent Schrödinger equation for infinite spherical quantum well are as follows. The Schrödinger equation in a spherical coordinator system is

$$-\frac{\hbar^2}{2m}\left[\frac{1}{r^2}\frac{\partial}{\partial r}\left(r^2\frac{\partial\psi}{\partial r}\right) + \frac{1}{r^2\sin\theta}\frac{\partial}{\partial\theta}\left(\sin\theta\frac{\partial\psi}{\partial\theta}\right) + \frac{1}{r^2\sin^2\theta}\frac{\partial^2\psi}{\partial\phi^2}\right] = [E - V(r)]\psi \tag{8}$$

The spherical quantum well boundary condition is

$$V(r) = \begin{cases} 0 & r < 0 \\ \infty & r \geq 0 \end{cases} \tag{9}$$

Solving the equation with the boundary condition, one obtains immediately the normalized wavefunctions for spherical coordinators as

$$\psi_{n,l,m}(r,\theta,\phi) = \sqrt{\frac{2}{a^3}}\frac{j_l(\beta_{nl}r)}{j_{l+1}(\beta_{nl})} Y_l^m(\vartheta,\phi) \tag{10}$$

where j_l represents a spherical Bessel function whose zero points are at β_{nl} and the spherical harmonics $Y_l^m(\vartheta,\phi)$ are composed with Legendre polynomials $P_l^m(\cos\theta)$ as well as normalized coefficients as

$$Y_l^m(\vartheta,\phi) = (-1)^m\sqrt{\frac{(2l+1)(l-m)!}{(l+m)!}}P_l^m(\cos\theta)e^{im\phi} \tag{11}$$

Undergoing the integration in angular coordinates θ and ϕ, and considering the spin degeneration 2, one obtains

$$\frac{n(r)}{n_0} = \frac{4}{3N}\sum_{nl}(2l+1)\left[\frac{j_l(\beta_{nl}r)}{j_{l+1}(\beta_{nl})}\right]^2 \tag{12}$$

where N represents the number of total electrons in the box. The eigenenergy corresponding to the wavefunction is obtained by

$$E_{nl} = \frac{\beta_{nl}^2\hbar^2}{2ma^2} \tag{13}$$

2.3. Quantum size effects on electron density and small particle plasmon

Let us now show some numerical results to confirm the above descriptions. We compare the electron density before and after incorporating the quantum size effects. In Figure 1, electron density is shown as a function of the radial coordinate.

One sees in Figure 1 that when the size of the particle is reduced, the intensity variation intensifies, which indicates there are significant changes due to quantum confinement. When the size of the particle increases, the quantum size effects become less pronounced. We have computed up to 8 nm. The intensity curve appears similar to the constant intensity shown by the dotted line, or the difference becomes unnoticeable. We take two notes as follows. First, the bigger the particle, the more electrons in the particle. The number of electrons augments dramatically with the size. Fortunately, one does not have to calculate too big particles, as the quantum size effects appear to vanish rapidly. Second, the parameter involved in the computation is the number of total electrons N, and the size is assessed from the density of the materials. The sizes marked in Figure 1 correspond to gold. For other materials, the density varies, and the size changes accordingly.

Let us now calculate the polarizability in Equation (6) using the density function shown in Figure 1. We choose to show the imaginary part, as it appears better for the eyes. In Figure 2, the imaginary part of the polarizability is shown.

As one can see in Figure 2, there is a significant blueshift with the decrease in particle size. In other words, there is a significant redshift when the particle size is increased. The strength is also decreased when the particle size is reduced, or the strength is increased when the size of the particle is increased. We take note as follows. When the particle size reduces to the extreme scale, there can hardly be plasmon resonance. There is no plasma, there

Figure 1
Normalized electron density $n(r)/n_0$ as a function of radial coordinate r/a for gold with various radii. The dotted line indicates the constant density $n(r)/n_0 = 1$, without taking into account the quantum size effects. The legend table in Figure 2 is shared with Figure 1

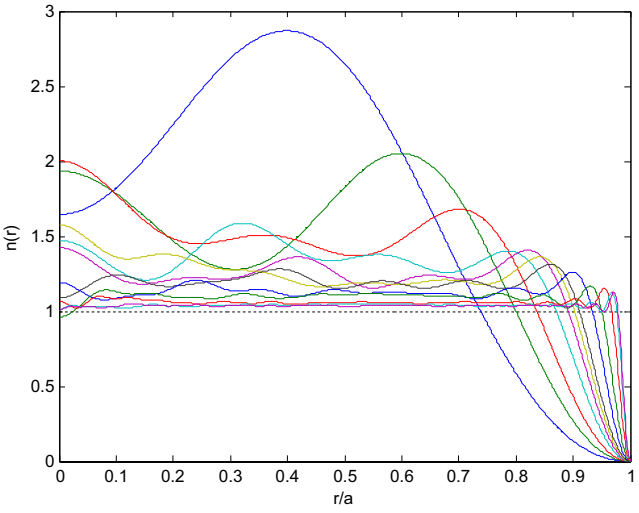

Figure 2
Imaginary part of polarizability as a function of normalized angular frequency ω/ω_p for various radii. The polarizability is normalized. The dotted line is for $n(r)/n_0 = 1$ which indicates the situation where the quantum size effects are not taken into account

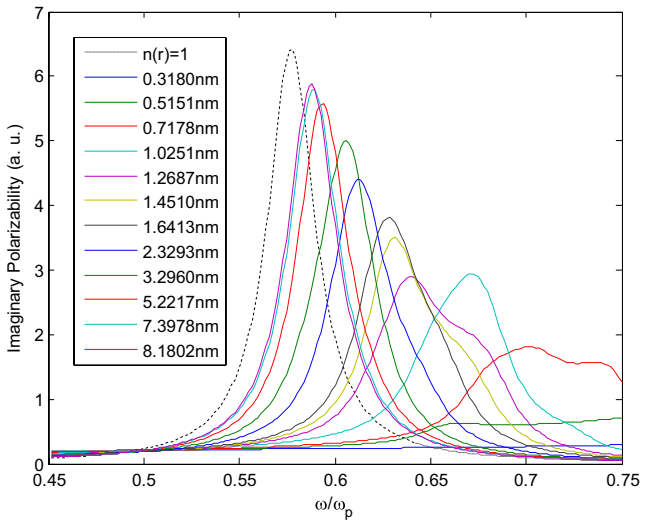

Figure 3
Small particle plasmon (a) strength and (b) spectral shift, as a function of the size of the particle. The angular frequency is normalized to the angular plasmon frequency. The dotted line in (a) represents the plasmon strength when $n(r)/n_0 = 1$, whereas the dotted line in (b) represents the plasmon angular frequency when $n(r)/n_0 = 1$

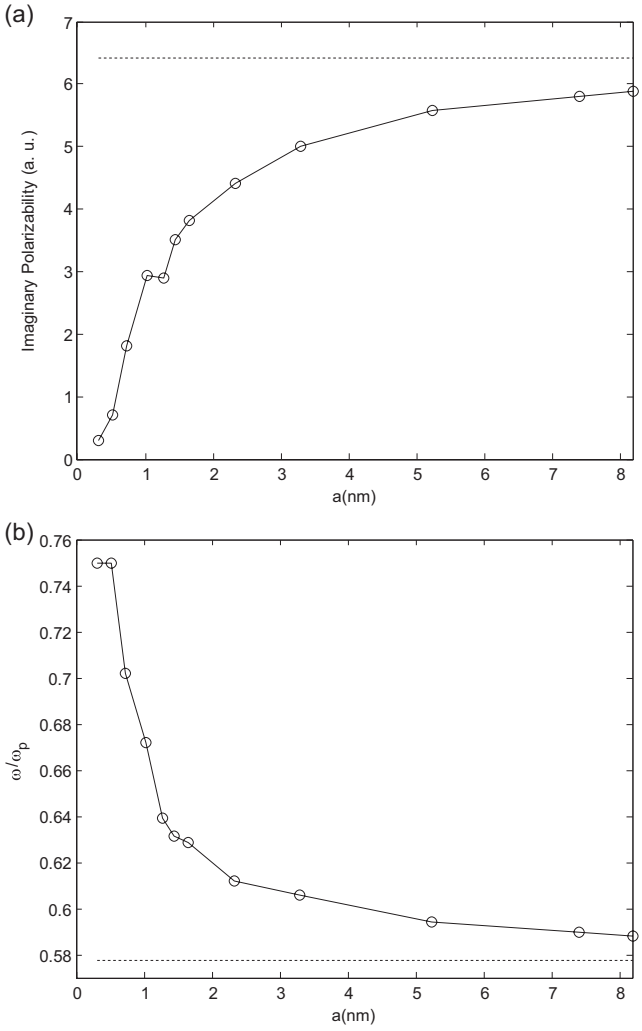

is no plasmon. The strength and spectral dependence are shown in Figure 3(a) and (b), respectively.

Figure 3(b) demonstrates the redshift we predicted. When the particle size increases, the plasmon frequency decreases. The trend is to move closer to the plasmon frequency that does not include the quantum size effects, that is, $\omega_{sp} \approx 0.577\omega_p$. As aforementioned, an increase in temperature causes the expansion of most materials. If the size of the quantum particle is augmented due to receiving heat, the quantum size effects can be manifested as a redshift in the plasmon absorption or radiation, which is referred to as the indirect thermal redshift.

The computation usually involves a very large number of electrons. In some cases, it is possible to find some sum rules so that the summation can be converted into integrals. On the other hand, in the process, the information about the quantum confinement may be smeared out or modified, so that the results would be less reliable for quantum particles where the number of carriers is not that big. In the present work, we adopt a scheme to take into account every electron. Since the particles we are interested in are rather small, we have been able to handle the computation on a supercomputer. Another issue of concern is the possible interband transitions. In the present work, the interband transitions are excluded. One can handle the intraband and interband transitions separately because the two frequency ranges usually do not overlap each other [31–36]. Therefore, as far as plasmonics is concerned, taking into account only the intraband transitions becomes adequate.

Emphasizing the intraband transition is particularly meaningful as far as the quantum size effects are involved. It may be seen as a fingerprint for the tiny effects because the band structures are not to be modified and the interband transitions remain intact as the entire band structure, that is, the density of states (DOS) map remains the same. Fluctuations in the intraband transitions cause changes in the collective movements of the intraband electrons, that is, the plasmon frequency shifts, which is what the present work is reporting. Keeping in mind the above criterion is useful and plausible while observing and identifying quantum size effects manifested by tiny shifts in plasmon spectra.

Finally, it is usually well-known that the damping effects are variant when the size of the particle decreases. However, in the computation, a constant number is used for the damping factor, which is to avoid having extra parameters simultaneously in the computation, so that the changes in plasmon frequency due to quantum size effects and temperature could be emphasized. Indeed, the damping changes mainly the shape of the plasmon peaks and has no significant impact on the plasmon frequency. Note in passing that surface reconstruction, lattice defects, and non-uniform strain can also affect plasmonic response and broaden peaks significantly. Our model does not include these fluctuations.

3. Experimental Evidence

In this section, we show a piece of experimental evidence for the redshift. Since the quantum size effects are so small, a near-field spectroscopy to observe the quantum size effects is unrealistic [23–28]. Spectral shifts in optical spectra have been seldomly reported, or reported without specific explanation (see, for

instance, references [7, 12] and the references therein). To find some experimental evidence, one has to resort to far-field optical spectroscopy on a collective sample in a large area.

Faujasite zeolites were synthesized. Zeolites are mesoporous materials and are widely used for catalysis. We synthesized the samples with a sol-gel technique [30]. The samples underwent many examinations with conventional tools, such as XRD, EDS, SEM, and TEM. The SEM and TEM images showed that a group of zeolite cells form agglomerates ~1.39 μm in size and the agglomerates construct layers whose thickness is ~0.12 μm. Optical spectroscopy in the ultraviolet and visible range has been carried out. Based on the resulting Tauc plots, band gaps can be estimated. The direct and indirect were evaluated to be 4.35 eV and 3.12 eV, respectively. For details of the synthesis and characterization, the readers are referred to Koop-Santa et al. [30], where the merits of the technique as well as the usefulness of the materials are extensively discussed.

The sample that is relevant to the present work underwent two different calcination temperatures, 90 °C and 450 °C. The sample under different temperatures was rather stable and showed a degree of mixture of crystallized octahedrons and morphologies. We have carried out optical spectroscopy for the sample at different calcination temperatures. Reflectance spectra cover UV-Vis were carried out with a UV-Vis-NIR spectrophotometer (Agilent, Cary 5000). The spectrophotometer was equipped with an integrating sphere in the wavelength range of 200 nm–800 nm. The optical spectra are recorded, namely FAU-90 and FAU-450, which indicate the different calcination temperatures.

Figure 4 shows the optical spectra of FAU-90 and FAU-450. One notices that the two spectra are almost identical, only that the spectrum TAU-450 is shifted a little towards a lower frequency, that is a redshift. Note that a longer wavelength means a lower frequency. The inserted figure in Figure 4 shows that the redshift is approximately 5 nm at around 244 nm in wavelength. Throughout the spectral range, the tiny redshift can also be observed.

It is reasonable to assess that the aforementioned quantum size effects take part in the redshift, as it stands for the aforementioned criterion that the quantum size effects would be manifested when the entire band structure remains intact and only a shift is present in the plasmon spectrum. Obviously, the band structure is not modified at all by the heating, or the heating is not yet destructive.

Figure 4
Optical absorption spectra for TAU-90 and TAU-450. The peak area is enlarged and inserted to show details

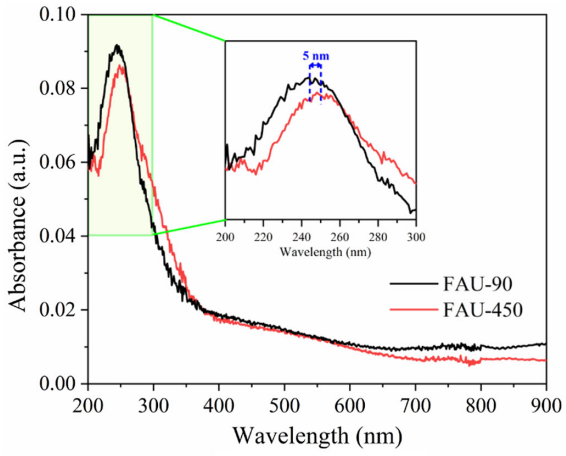

The stability of the materials has also been consistent with SEM and TEM images. The heating contributes only to the expansion of all objects in size.

The band structure of zeolite molecules is usually complicated [31–41]. Hundreds of atoms bound together to form a complex molecule, including many metallic atoms. Nevertheless, the complex molecule is a quantum system under quantum confinement, similar to a quantum particle. Therefore, one generalizes the situation to reach reasonable conclusions as follows. Since the spectrum is not modified, the sample keeps all components and structures. The heat causes only expansion in size. The interband transition is not a part of the change, as the spectrum is intact. There remain only intraband movements. The electrons are moving within the intact DOS map, which is indeed a collective movement of plasma, and would bring about changes in plasmons. In other words, the quantum size effects described in the present work are a leading reason for the redshift observed in our experiment. One may think of other possible reasons for the redshift. However, since the fact that the spectrum is intact, any destructive incidence does not occur. Only the electric movements within the stable band structure are responsible for the tiny redshift. Our numerical modeling provides the background in quantum mechanics to support the mechanism. The thermal redshift is caused by the temperature-induced quantum size effects.

In terminating, we take some notes on possible improvements to our experiments. So far, we are unable to carry out in situ measurements to obtain a continuous spectrum. Details on the sample preparation and characterization can be found in Koop-Santa et al. [30]. Since the experiments were conducted for collective samples, it was hard to assert sample properties, such as the size, shape, structure, etc, Microscopy and spectroscopy performed for individual particles would reveal the missing information. The fine work is beyond our ability and has not been reported even remotely related to the redshift that is handled in the present work. In addition, it would be nice to have an error analysis. The types of equipment involved in the work cited in the present work. Finally, we are unaware of any reports of redshifts for metallic or semiconductor materials. The work requires tremendous effects.

4. Conclusion and Perspective

In conclusion, we have studied the spectral redshift with the increase in temperature on quantum particles. A model is established based on quantum mechanics to deal with the small particle plasmon. Possible thermal redshifts have been predicted to be caused indirectly by the quantum size effects. If quantum particles are heated, the size of the particles is enlarged, and consequently, the quantum size effects modify the plasmon but not the band structure. Therefore, the redshift is caused indirectly by the heat via quantum size effects. It has been modeled for gold quantum particles, and the simulation can be extended to other metals and semiconductors. The results are also instructive to other quantum systems, such as complex molecules and their mesoscopic aggregators. A key scheme is that every electron inside the quantum particle is taken into account. Tiny quantum size effects are harvested, and the redshift becomes significant. Phenomenological experimental evidence is also given for the spectral redshift. Crystalized and layered Faujasite zeolites were synthesized. Zeolites are mesoscopic porous materials and are widely used for catalysis. The samples were characterized with the most conventional tools. Optical spectroscopy has been carried out from ultraviolet to visible, and the resulting spectra show a significant redshift with the increase in temperature.

It is reasonable to assess that the quantum size effects are responsible for the redshift because the band structure is not modified at all by the heating. The band structure of zeolite molecules is usually complicated [31–41]. Hundreds of atoms bound together to form a complex molecule, including many metallic atoms. Nevertheless, the complex molecule is a quantum system, similar to a quantum particle. Therefore, one generalizes the situation to reach reasonable conclusions as follows. Since the spectrum is not modified, the sample keeps all components and structures. The heat causes only expansion in size. The interband transition is not a part of the change, as the spectrum is intact. There remain only intraband movements. The electrons are moving within the same DOS map, which is indeed a collective movement of plasma, and would bring about plasmons. In other words, the quantum size effects described in the present work are a strong reason for the redshift observed in our experiment. One may think of other possible reasons for the redshift. However, since the fact that the spectrum is intact, any destructive incidence does not occur. Only the electric movements within the stable band structure are responsible for the tiny redshift. Our numerical modeling provides the background in quantum mechanics for the mechanism. The thermal redshift is caused by the temperature-induced quantum size effects.

Acknowledgment

We gratefully acknowledge the funding provided by DGAPA-PAPIIT Grant IG101623.

Ethical Statement

This study does not contain any studies with human or animal subjects performed by any of the authors.

Conflicts of Interest

The authors declare that they have no conflicts of interest to this work.

Data Availability Statement

Data sharing is not applicable to this article as no new data were created or analyzed in this study.

Author Contribution Statement

Mufei Xiao: Conceptualization, Methodology, Software, Validation, Formal analysis, Investigation, Resources, Data curation, Writing – original draft, Writing – review & editing, Visualization, Supervision, Project administration, Funding acquisition. **Constanza Koop-Santa:** Validation, Formal analysis, Investigation, Resources, Data curation. **Nikifor Rakov:** Validation, Formal analysis, Investigation, Resources, Data curation.

References

[1] Lv, C., Meng, F., Cui, L., Jiao, Y., Jia, Z., Qin, W., & Qin, G. (2024). Voltage-controlled nonlinear optical properties in gold nanofilms via electrothermal effect. *Nature Communications*, *15*(1), 6372. https://doi.org/10.1038/s41467-024-50665-7

[2] de Renzi, V., Betti, M. G., & Mariani, C. (1993). Quantum size effects and temperature dependence of low-energy electronic excitations in thin Bi crystals. *Physical Review B*, *48*(7), 4767–4776. https://doi.org/10.1103/PhysRevB.48.4767

[3] Pan, C., Tong, Y., Qian, H., Krasavin, A. V., Li, J., Zhu, J., . . . , & Wang, P. (2024). Large area single crystal gold of single nanometer thickness for nanophotonics. *Nature Communications*, *15*(1), 2840. https://doi.org/10.1038/s41467-024-47133-7

[4] Novo, C., Funston, A. M., & Mulvaney, P. (2008). Direct observation of chemical reactions on single gold nanocrystals using surface plasmon spectroscopy. *Nature Nanotechnology*, *3*(10), 598–602. https://doi.org/10.1038/nnano.2008.246

[5] Scholl, J. A., Koh, A. L., & Dionne, J. A. (2012). Quantum plasmon resonances of individual metallic nanoparticles. *Nature*, *483*(7390), 421–427. https://doi.org/10.1038/nature10904

[6] Coviello, V., Badocco, D., Pastore, P., Fracchia, M., Ghigna, P., Martucci, A., . . . , & Amendola, V. (2024). Accurate prediction of the optical properties of nanoalloys with both plasmonic and magnetic elements. *Nature Communications*, *15*(1), 834. https://doi.org/10.1038/s41467-024-45137-x

[7] Aflalo, K., Gao, P., Trivedi, V., Sanjeev, A., & Zalevsky, Z. (2024). Optical super-resolution imaging: A review and perspective. *Optics and Lasers in Engineering*, *183*, 108536. https://doi.org/10.1016/j.optlaseng.2024.108536

[8] Zhou, J., Zhang, X., Xu, X., Wei, Y., Zhang, T., Tang, F., . . . , & Hu, M. (2025). Single-bacterium diagnosis via terahertz near-field dielectric nanoimaging. *ACS Applied Materials & Interfaces*, *17*(12), 18074–18082. https://doi.org/10.1021/acsami.4c22571

[9] Kotkar, M. T., Wani, S. M., Shinde, P. G., Patil, A. G., & Jadhav, K. M. (2025). Preparation and thermophysical investigations of water and ethylene glycol based CuO nanofluid using cationic CTAB surfactant for heat transfer application. *Solid State Communications*, *400*, 115914. https://doi.org/10.1016/j.ssc.2025.115914

[10] Jin, X., Cui, Y., Chen, H., Hao, R., & Zhang, F. (2025). High quality surface plasmon resonance microscopy based on dual-channel frequency-domain filtering method. *Optics & Laser Technology*, *183*, 112311. https://doi.org/10.1016/j.optlastec.2024.112311

[11] Ji, S., Guo, J., Li, Z., Tong, L., Guo, J., Liu, J., . . . , & Fu, X. (2025). Development of a femtosecond analytical electron microscopy based on a Schottky field emission transmission electron microscope. *Review of Scientific Instruments*, *96*(3), 033701. https://doi.org/10.1063/5.0226913

[12] Jäckering, L., Wirth, K. G., Conrads, L., Profe, J. B., Rothstein, A., Kyoseva, H., . . . , & Taubner, T. (2025). Super-resolution imaging of nanoscale inhomogeneities in hBN-covered and encapsulated few-layer graphene. *Advanced Science*, *12*(14), 2409039. https://doi.org/10.1002/advs.202409039

[13] Khajuria, P., Sharma, V. D., Kumar, I., Khajuria, A., Prakash, R., & Choudhary, R. J. (2025). Optoelectronic properties of $Na_2ZrO_3:Eu^{3+}$ phosphor: Judd-Ofelt insights and applications in solid-state lighting and latent fingerprinting. *Journal of Alloys and Compounds*, *1025*, 180268. https://doi.org/10.1016/j.jallcom.2025.180268

[14] Fan, Y., Xue, X., Yang, F., Zhao, J., Xiong, X., Sun, J., . . . , & Zhang, Z. (2023). Reconstruction of the near-field electric field by snom measurement. *Nano Letters*, *23*(21), 9900–9906. https://doi.org/10.1021/acs.nanolett.3c02833

[15] Kwon, S., Oh, M. J., Lee, S., Lee, G., Jung, I., Oh, M., & Park, S. (2023). Au octahedral nanosponges: 3D plasmonic nanolenses for near-field focusing. *Journal of the American Chemical Society*, *145*(50), 27397–27406. https://doi.org/10.1021/jacs.3c08315

[16] Matson, J., Wasserroth, S., Ni, X., Obst, M., Diaz-Granados, K., Carini, G., . . . , & Caldwell, J. D. (2023). Controlling the propagation asymmetry of hyperbolic shear polaritons in

beta-gallium oxide. *Nature Communications*, *14*(1), 5240. https://doi.org/10.1038/s41467-023-40789-7

[17] Maciel-Escudero, C., Yankovich, A. B., Munkhbat, B., Baranov, D. G., Hillenbrand, R., Olsson, E., . . . , & Shegai, T. O. (2023). Probing optical anapoles with fast electron beams. *Nature Communications*, *14*(1), 8478. https://doi.org/10.1038/s41467-023-43813-y

[18] Buscho, S. E., Xia, F., Shi, S., Lin, J. L., Szczesny, B., Zhang, W., . . . , & Liu, H. (2023). Non-invasive evaluation of retinal vascular alterations in a mouse model of optic neuritis using laser speckle flowgraphy and optical coherence tomography angiography. *Cells*, *12*(23), 2685. https://doi.org/10.3390/cells12232685

[19] Lu, X., Wang, X., Wang, S., & Ding, T. (2023). Polarization-directed growth of spiral nanostructures by laser direct writing with vector beams. *Nature Communications*, *14*(1), 1422. https://doi.org/10.1038/s41467-023-37048-0

[20] Long, L., Deng, Q., Huang, R., Li, J., & Li, Z. Y. (2023). 3D printing of plasmonic nanofocusing tip enabling high resolution, high throughput and high contrast optical near-field imaging. *Light: Science & Applications*, *12*(1), 219. https://doi.org/10.1038/s41377-023-01272-6

[21] Thomaschewski, M., Prämassing, M., Schill, H. J., Zenin, V. A., Bozhevolnyi, S. I., Sorger, V. J., & Linden, S. (2023). Near-field observation of the photonic spin hall effect. *Nano Letters*, *23*(24), 11447–11452. https://doi.org/10.1021/acs.nanolett.3c02829

[22] Wang, Z., Liu, F., Cui, K., Feng, X., Zhang, W., & Huang, Y. (2024). First-principles study of charge-transfer-plasmon-enhanced photoemission from a gold-nanoparticle–sodium-atom emitter. *Physical Review A*, *109*(4), 043119. https://doi.org/10.1103/PhysRevA.109.043119

[23] Zhang, Q., Rosa, R. S. L., Ray, A., Durlet, K., Dorrazehi, G. M., Bernardi, R. C., & Alsteens, D. (2025). Probing SARS-CoV-2 membrane binding peptide via single-molecule AFM-based force spectroscopy. *Nature Communications*, *16*(1), 6. https://doi.org/10.1038/s41467-024-55358-9

[24] Cheppali, S. K., Li, C., Xing, W., Sun, R., Yang, M., Xue, Y., . . . , & Sui, S. F. (2025). Single-molecule two- and three-colour FRET studies reveal a transition state in SNARE disassembly by NSF. *Nature Communications*, *16*(1), 250. https://doi.org/10.1038/s41467-024-55531-0

[25] Wang, Y., Ye, J., Liu, X., Zhang, Z., Shang, F., Qi, X., . . . , & Le, S. (2025). Mechanically weak and highly dynamic state of mechanosensitive titin Ig domains induced by proline isomerization. *Nature Communications*, *16*(1), 2771. https://doi.org/10.1038/s41467-025-57989-y

[26] Aris, K. D. P., Cofsky, J. C., Shi, H., Al-Sayyad, N., Ivanov, I. E., Balaji, A., . . . , & Bryant, Z. (2025). Dynamic basis of supercoiling-dependent DNA interrogation by Cas12a via R-loop intermediates. *Nature Communications*, *16*(1), 2939. https://doi.org/10.1038/s41467-025-57703-y

[27] Yuan, F., Qi, H., Song, B., Cui, Y., Zhang, J., Liu, H., . . . , & Liu, T. (2025). Tailorable biosensors for real-time monitoring of stress distribution in soft biomaterials and living tissues. *Nature Communications*, *16*(1), 1081. https://doi.org/10.1038/s41467-025-56422-8

[28] Pérez-Sánchez, J. B., & Yuen-Zhou, J. (2025). Radiative pumping vs vibrational relaxation of molecular polaritons: A bosonic mapping approach. *Nature Communications*, *16*(1), 3151. https://doi.org/10.1038/s41467-025-58045-5

[29] Xiao, M., & Rakov, N. (2015). Size and temperature dependent plasmons of quantum particles. *International Journal of Modern Physics B*, *29*(21), 1550146. https://doi.org/10.1142/S0217979215501465

[30] Koop-Santa, C., Yocupicio-Gaxiola, R. I., Murrieta-Rico, F. N., Avalos-Borja, M., Xiao, M., Petranovskii, V., & Reyes-Serrato, A. (2024). Additive-free synthesis of layer-like Faujasite-type zeolite X. *Journal of Materials Science*, *59*(23), 10169–10181. https://doi.org/10.1007/s10853-024-09739-6

[31] Jackson, J. D. (1999). *Classical electrodynamics* (3rd ed.). USA: Wiley.

[32] Keller, O. (1994). Optical polarizability of small quantum particles: Local-field effects in a self-field approach. *Journal of the Optical Society of America B*, *11*(8), 1480–1489. https://doi.org/10.1364/JOSAB.11.001480

[33] Maalmarugan, J., Ferin, R. Z., Joesna, G., Mustafa, A., Mohamed, M. G., Bououdina, M., . . . , & SenthilKannan, K. (2022). In situ grown ZnO nanoparticles using *Begonia* leaves–dielectric, magnetic, filter utility and tribological properties for mechano-electronic applications. *Applied Physics A*, *128*(3), 217. https://doi.org/10.1007/s00339-022-05371-w

[34] Saravanan, P., SenthilKannan, K., Mustafa, A., Vimalan, M., Bououdina, M., Balasubramanian, S., . . . , & Tamilselvan, S. (2021). Dielectric and magnetic properties of *Allium cepa* and *Raphanus sativus* extracts biogenic ZnO nanoparticles. *Journal of Materials Science: Materials in Electronics*, *32*(1), 590–603. https://doi.org/10.1007/s10854-020-04841-2

[35] Sansonetti, J. E., Mullin, D. P., Dixon, J. R., & Furdyna, J. K. (1979). Electron paramagnetic resonance in powdered semiconductors and semimetals. *Journal of Applied Physics*, *50*(8), 5431–5441. https://doi.org/10.1063/1.326593

[36] Su, L., Douglas, A., Szurek, M., Hébert, A. H., Krahn, A., Groth, R., . . . , & Greiner, M. (2025). Fast single atom imaging for optical lattice arrays. *Nature Communications*, *16*(1), 1017. https://doi.org/10.1038/s41467-025-56305-y

[37] Chen, S. H., Ko, Y. C., Huang, Y. C., He, X. R., Liang, H. C., & Chiang, H. P. (2025). Fabrication and application of periodic silver hollow nanorod arrays for enhanced photoluminescence. *Chinese Journal of Physics*, *95*, 74–81. https://doi.org/10.1016/j.cjph.2025.02.036

[38] Radhakrishnan, R. C., James, A. M., Das K, R., Balendra, & Thomas, J. (2025). Fluorescent zinc sulphate based hybrid solid exhibiting "Turn-off" switching towards H_2O_2. *Journal of Molecular Structure*, *1334*, 141804. https://doi.org/10.1016/j.molstruc.2025.141804

[39] Sapchenko, S. A., Belosludov, R. V., Vitoria-Irezabal, I. J., da Silva, I., Chen, X., Whitehead, G. F. S., . . . , & Schröder, M. (2025). Direct synthesis of a semiconductive double-helical phosphorus allotrope in a metal-organic framework. *Nature Communications*, *16*(1), 1578. https://doi.org/10.1038/s41467-025-55999-4

[40] Dou, Y., Geng, C., Duan, C., Hu, S., Deng, X., Chen, Y., . . . , & Ku, Z. (2025). A vapor-assisted annealing strategy towards high-quality perovskite absorbers enabling efficient wide bandgap perovskite solar cells. *Nano Energy*, *139*, 110914. https://doi.org/10.1016/j.nanoen.2025.110914

[41] Bensassi, L., Triki-Baara, F., Megrouss, Y., Drim, K., Chouaih, A., Saidj, M., . . . , & Hatzidimitriou, A. (2025). Design, synthesis, characterization, NCI-RDG, Hirshfeld surface analysis, chemical reactivity and quantum chemical calculations of Z-3-N-ethyl-2-N-[(2-methoxyphenyl) imino] thiazolidin-4-one. *Journal of Molecular Structure*, *1328*, 141301. https://doi.org/10.1016/j.molstruc.2024.141301

How to Cite: Xiao, M., Koop-Santa, C., & Rakov, N. (2025). Redshift of Quantum-Particle Plasmon Stemming from Thermal-Induced Quantum Size Effects: Numerical Modeling and Experimental Evidence. *Journal of Optics and Photonics Research*. https://doi.org/10.47852/bonviewJOPR52025955